Supporting Information for Evaluating Nirmatrelvir Resistance in SARS-CoV-2 Main Protease: A Comparison Between MM/PBSA and Free Energy Perturbation

Xiaoxiao Lyu[†] and Ye Mei[*,†,‡,¶]

†*State Key Laboratory of Precision Spectroscopy, School of Physics and Electronic Science, East China Normal University, Shanghai 200241, China*

‡*NYU-ECNU Center for Computational Chemistry at NYU Shanghai, Shanghai 200062, China*

¶*Collaborative Innovation Center of Extreme Optics, Shanxi University, Taiyuan, Shanxi 030006, China*

E-mail: samuel.y.mei@gmail.com

Table S1: Hydrogen bonding analysis for the production simulation of wild-type M^{pro}-Nirmatrelvir complex.

No.	Acceptor	DonorH	Donor	Frames	Frac	AvgDist	AvgAng
1	4WI_613@O3	GLU_166@H	GLU_166@N	99732	1.00	2.98	164.03
2	GLU_166@O	4WI_613@H30	4WI_613@N5	98772	0.99	2.92	163.18
3	HIE_164@O	4WI_613@H29	4WI_613@N4	80127	0.80	3.03	160.87
4	4WI_613@O1	HIE_163@HE2	HIE_163@NE2	72678	0.72	2.87	150.96
5	4WI_613@N1	CYS_145@H	CYS_145@N	51082	0.51	3.24	154.62
6	4WI_613@O4	THR_190@H	THR_190@N	40409	0.40	3.11	159.05
7	PHE_140@O	4WI_613@H28	4WI_613@N2	38979	0.39	3.11	148.79
8	GLU_166@OE1	4WI_613@H28	4WI_613@N2	21044	0.21	3.06	147.03
9	4WI_613@N1	GLY_143@H	GLY_143@N	18509	0.19	3.13	146.77
10	GLU_166@OE2	4WI_613@H28	4WI_613@N2	17165	0.17	3.06	146.65

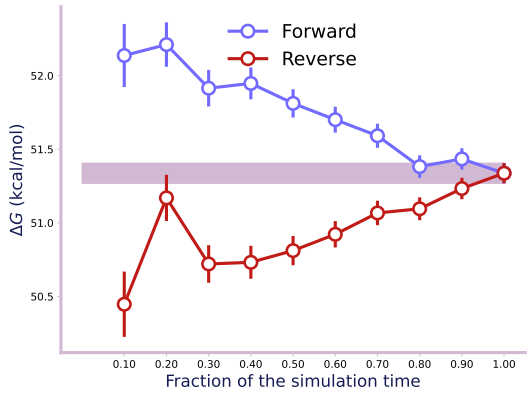

(A) A convergence plot for the consistency check of forward and backward free energy calculations over time.

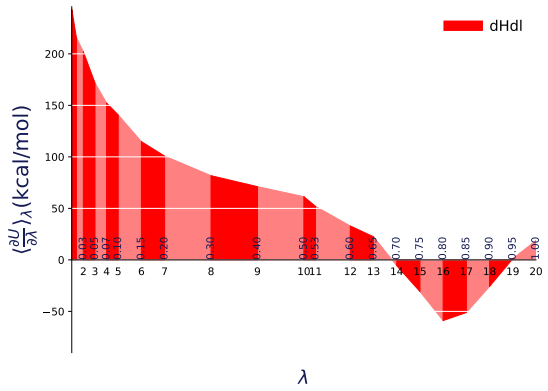

(B) A plot of $\langle \frac{\partial U}{\partial \lambda} \rangle$ versus λ for TI.

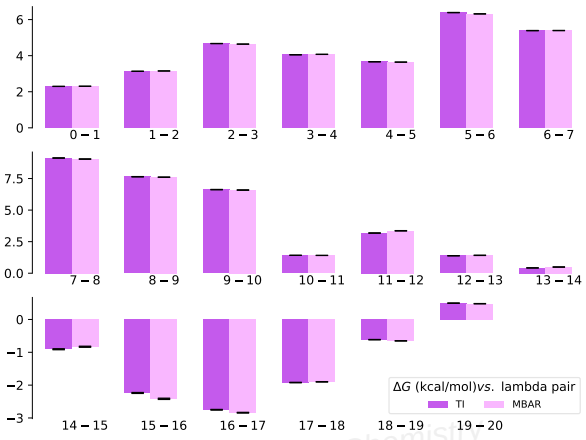

(C) A bar plot comparing free energy differences between adjacent states using TI and MBAR methods, including corresponding error estimates for each method.

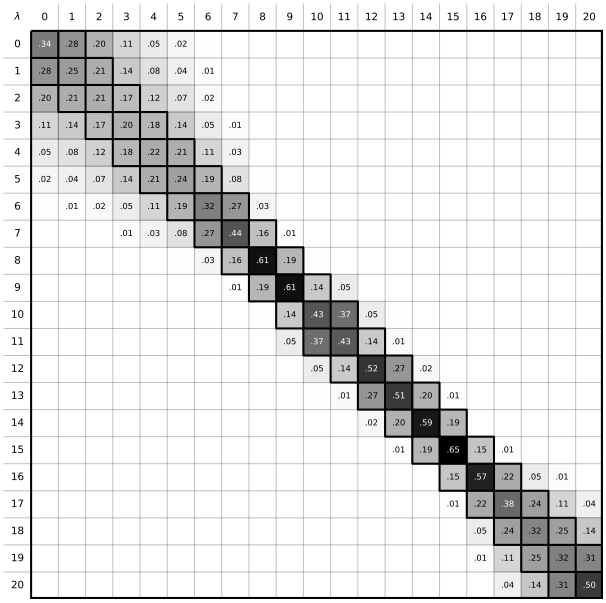

(D) An overlap matrix quantifies the overlap between potential energy difference distributions, ensuring accurate free energy calculations, with at least a tridiagonal structure required to interconnect terminal states (e.g., states 0 and 20).

Figure S1: Free energy convergence analysis is visualized using alchemlyb software, following established guidelines which provides a valuable consistency check,[1] with example plots illustrating the alchemical transformation substage simulations for $\Delta G^{\text{decouple}}_{\text{site}}$ for the wild-type M^{pro}-Nirmatrelvir complex.

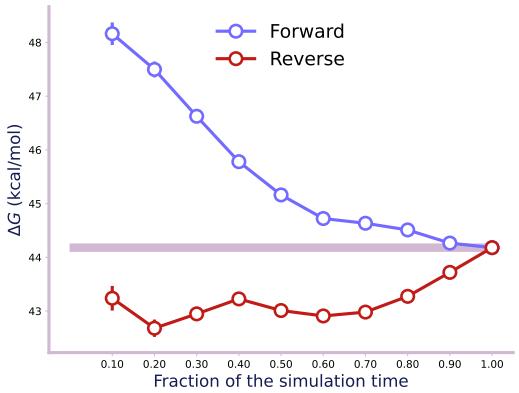

(A) A convergence plot for the consistency check of forward and backward free energy calculations over time.

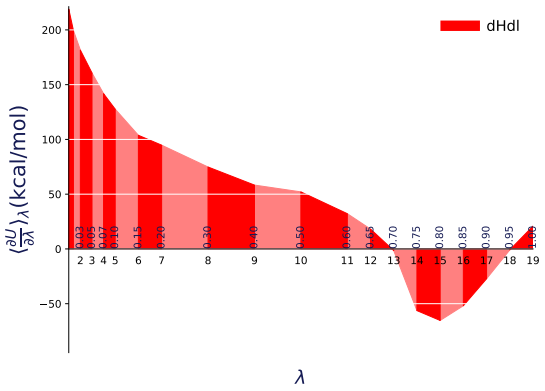

(B) A plot of $\langle \frac{\partial U}{\partial \lambda} \rangle$ versus λ for TI.

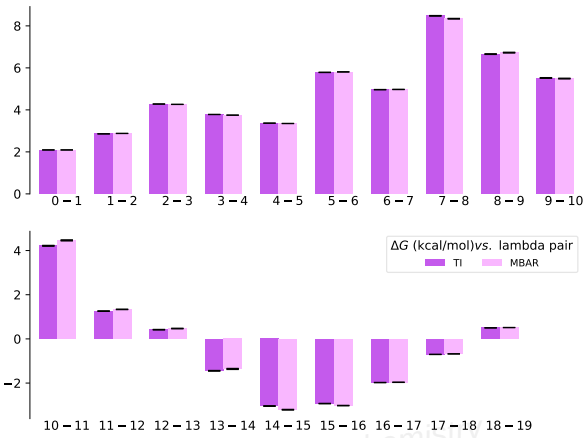

(C) A bar plot comparing free energy differences between adjacent states using TI and MBAR methods, including corresponding error estimates for each method.

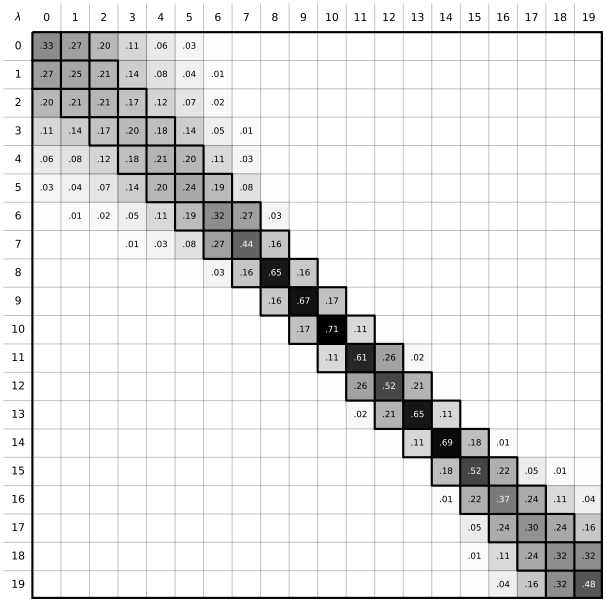

(D) An overlap matrix quantifies the overlap between potential energy difference distributions, ensuring accurate free energy calculations, with at least a tridiagonal structure required to interconnect terminal states (e.g., states 0 and 19).

Figure S2: Free energy convergence analysis is visualized using alchemlyb software, following established guidelines which provides a valuable consistency check,[1] with example plots illustrating the alchemical transformation substage simulations for $\Delta G^{\text{decouple}}_{\text{site}}$ for the SER144ALA M^{pro}-Nirmatrelvir complex.

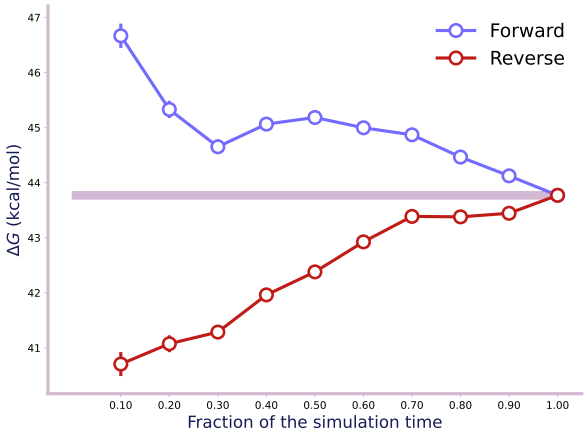

(A) A convergence plot for the consistency check of forward and backward free energy calculations over time.

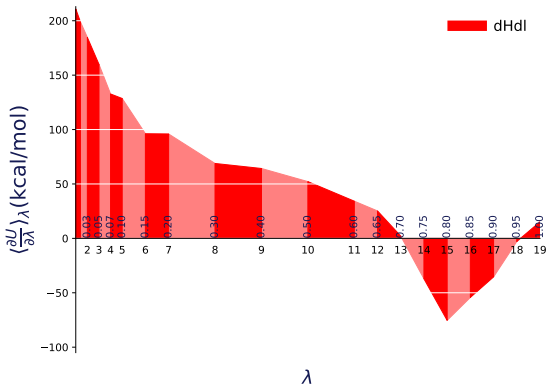

(B) A plot of $\langle \frac{\partial U}{\partial \lambda} \rangle$ versus λ for TI.

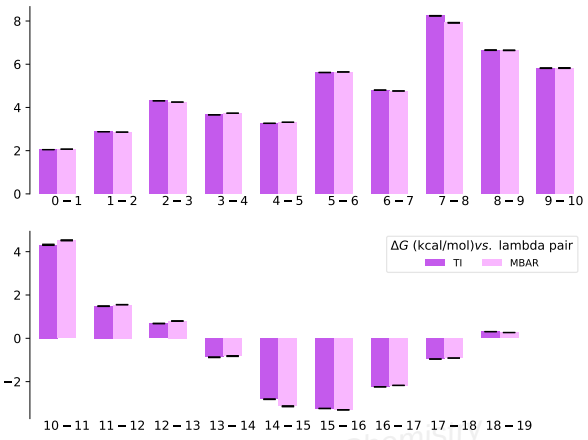

(C) A bar plot comparing free energy differences between adjacent states using TI and MBAR methods, including corresponding error estimates for each method.

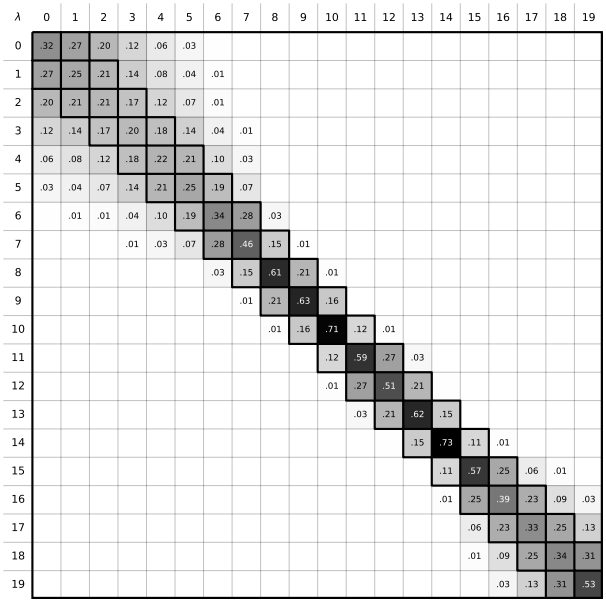

(D) An overlap matrix quantifies the overlap between potential energy difference distributions, ensuring accurate free energy calculations, with at least a tridiagonal structure required to interconnect terminal states (e.g., states 0 and 19).

Figure S3: Free energy convergence analysis is visualized using alchemlyb software, following established guidelines which provides a valuable consistency check,[1] with example plots illustrating the alchemical transformation substage simulations for $\Delta G^{\text{decouple}}_{\text{site}}$ for the MET165ALA M^{pro}-Nirmatrelvir complex.

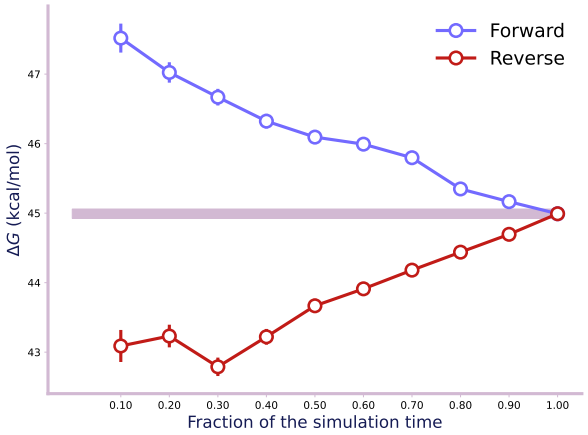

(A) A convergence plot for the consistency check of forward and backward free energy calculations over time.

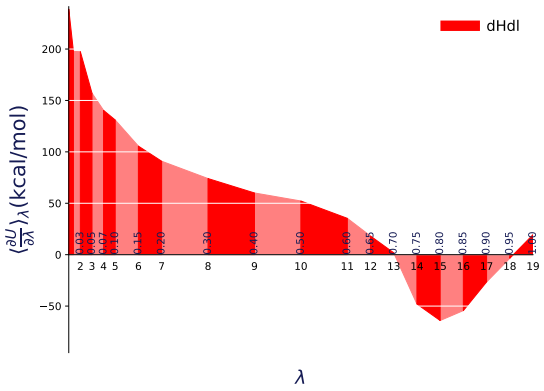

(B) A plot of $\langle \frac{\partial U}{\partial \lambda} \rangle$ versus λ for TI.

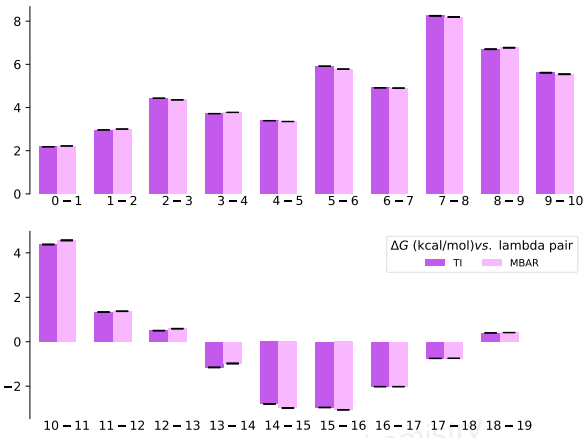

(C) A bar plot comparing free energy differences between adjacent states using TI and MBAR methods, including corresponding error estimates for each method.

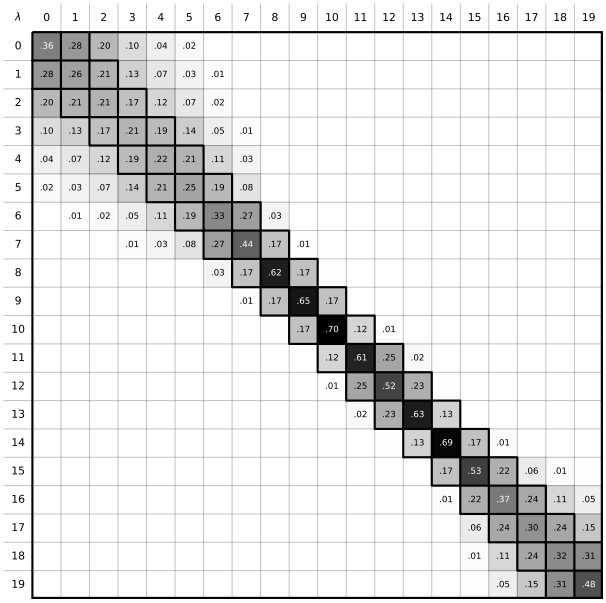

(D) An overlap matrix quantifies the overlap between potential energy difference distributions, ensuring accurate free energy calculations, with at least a tridiagonal structure required to interconnect terminal states (e.g., states 0 and 19).

Figure S4: Free energy convergence analysis is visualized using alchemlyb software, following established guidelines which provides a valuable consistency check,[1] with example plots illustrating the alchemical transformation substage simulations for $\Delta G^{\text{decouple}}_{\text{site}}$ for the GLU166ALA M^{pro}-Nirmatrelvir complex.

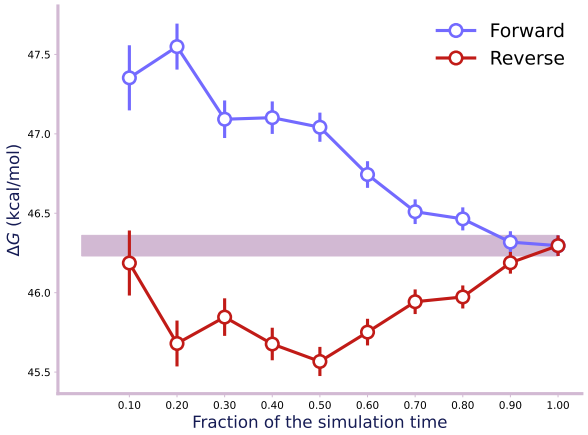

(A) A convergence plot for the consistency check of forward and backward free energy calculations over time.

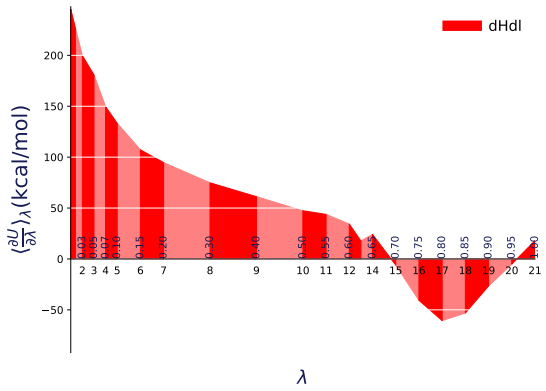

(B) A plot of $\langle \frac{\partial U}{\partial \lambda} \rangle$ versus λ for TI.

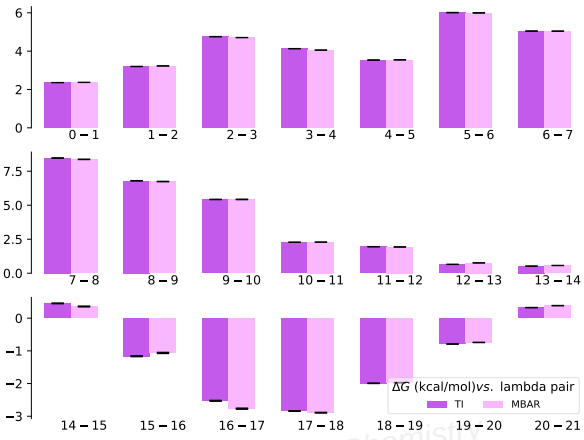

(C) A bar plot comparing free energy differences between adjacent states using TI and MBAR methods, including corresponding error estimates for each method.

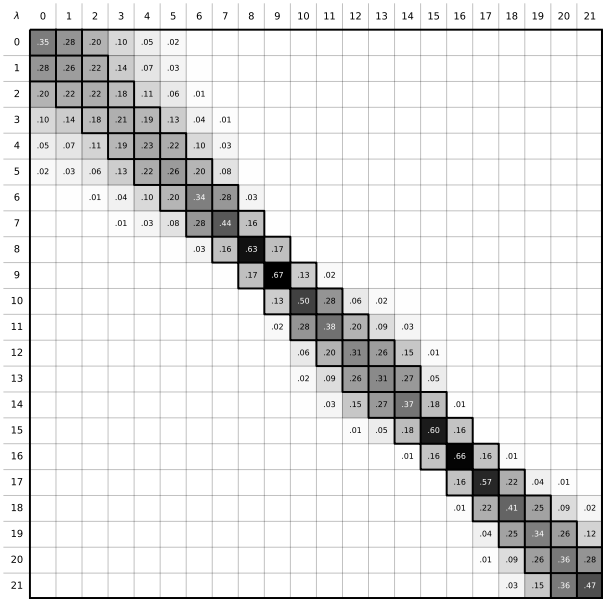

(D) An overlap matrix quantifies the overlap between potential energy difference distributions, ensuring accurate free energy calculations, with at least a tridiagonal structure required to interconnect terminal states (e.g., states 0 and 21).

Figure S5: Free energy convergence analysis is visualized using alchemlyb software, following established guidelines which provides a valuable consistency check,[1] with example plots illustrating the alchemical transformation substage simulations for $\Delta G^{\text{decouple}}_{\text{site}}$ for the HIE172ALA M^{pro}-Nirmatrelvir complex.

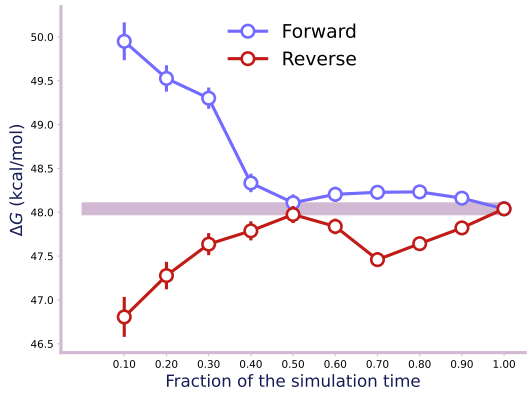

(A) A convergence plot for the consistency check of forward and backward free energy calculations over time.

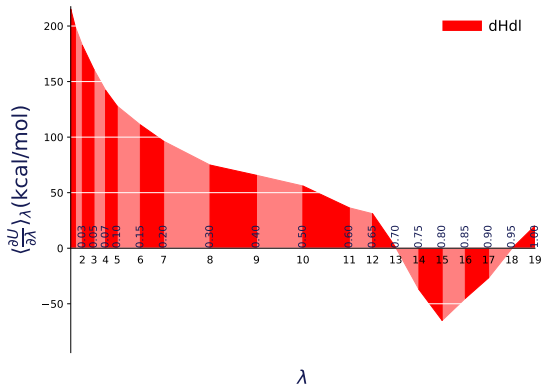

(B) A plot of $\langle \frac{\partial U}{\partial \lambda} \rangle$ versus λ for TI.

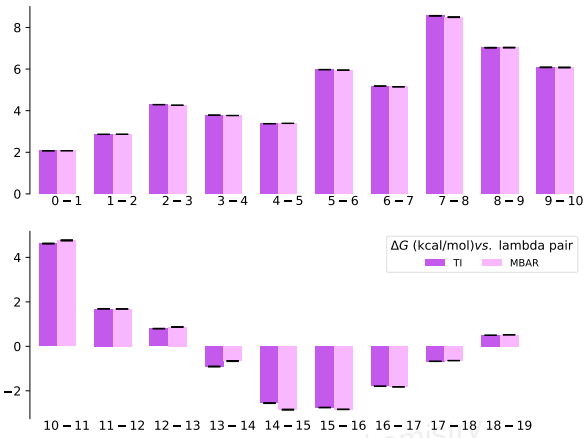

(C) A bar plot comparing free energy differences between adjacent states using TI and MBAR methods, including corresponding error estimates for each method.

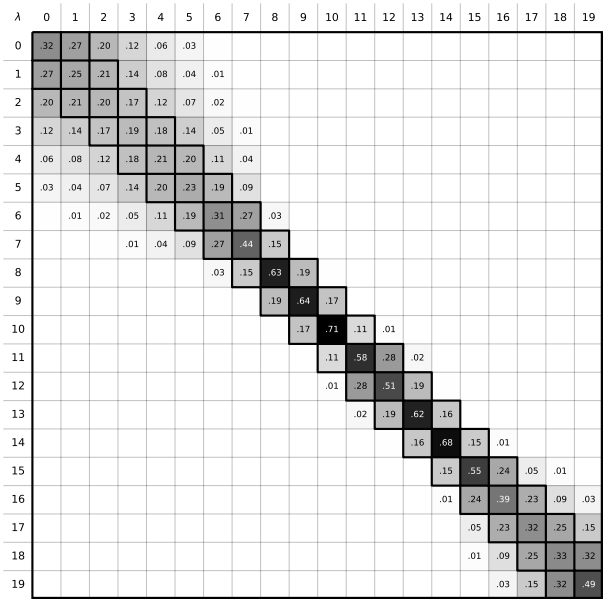

(D) An overlap matrix quantifies the overlap between potential energy difference distributions, ensuring accurate free energy calculations, with at least a tridiagonal structure required to interconnect terminal states (e.g., states 0 and 19).

Figure S6: Free energy convergence analysis is visualized using alchemlyb software, following established guidelines which provides a valuable consistency check,[1] with example plots illustrating the alchemical transformation substage simulations for $\Delta G^{\text{decouple}}_{\text{site}}$ for the GLN192ALA M^{pro}-Nirmatrelvir complex.

Table S2: Results measured by the Pearson correlation coefficient ($R_{\mathbf{Pearson}}$) between the predicted binding free energy values obtained from MM/PBSA, FEP (MBAR), and FEP (TI) calculations, and the corresponding experimental data.

Variant	Experiment	MM/PBSA	FEP (MBAR)	FEP (TI)
WILD	-11.92 ± 0.05	-46.11 ± 0.23	-12.84 ± 0.96	-12.54 ± 0.73
SER144ALA	-10.16 ± 0.03	-40.62 ± 0.24	-9.26 ± 0.70	-8.80 ± 0.73
MET165ALA	-10.42 ± 0.02	-38.82 ± 0.20	-8.23 ± 0.60	-8.06 ± 0.53
GLU166ALA	-9.63 ± 0.02	-45.08 ± 0.23	-9.43 ± 0.29	-8.97 ± 0.38
HIE172ALA	-9.11 ± 0.02	-41.11 ± 0.20	-9.63 ± 0.82	-9.45 ± 0.88
GLN192ALA	-9.88 ± 0.03	-49.27 ± 0.23	-11.81 ± 0.54	-11.42 ± 0.47
$R_{Pearson}$	-	0.18	0.56	0.57

References

(1) Klimovich, P. V.; Shirts, M. R.; Mobley, D. L. Guidelines for the analysis of free energy calculations. *J. Comput.-Aided Mol. Des.* **2015**, *29*, 397–411.

Communications in Computational Chemistry